Japanese Journal of Applied Physics

The Japan Society of Applied Physics

REGULAR PAPER

Lithium niobate single crystal thin film resonator with benzocyclobutene as a reflective layer

To cite this article: Ying Xing *et al* 2020 *Jpn. J. Appl. Phys.* **59** 016502

Japanese Journal of Applied Physics **59**, 016502 (2020)
https://doi.org/10.7567/1347-4065/ab6001

REGULAR PAPER

Lithium niobate single crystal thin film resonator with benzocyclobutene as a reflective layer

Ying Xing[1], Yao Shuai[1*], Xiaoyuan Bai[1], Lu Lv[1], Wenbo Luo[1], Chuangui Wu[1], Huizhong Zeng[1], Tao Yang[2], and Wanli Zhang[1]

[1]*State Key Laboratory of Electronic Thin Films and Integrated Devices, University of Electronic Science and Technology of China, Chengdu 610054, People's Republic of China*
[2]*School of Electronic Science and Engineering, University of Electronic Science and Technology of China, Chengdu 610054, People's Republic of China*

*E-mail: yshuai@uestc.edu.cn

Received August 10, 2019; revised November 28, 2019; accepted December 8, 2019; published online January 3, 2020

The intrinsic electromechanical coupling coefficient (k_t^2) of the piezoelectric material is the decisive factor limiting the band width of the thin film bulk acoustic (FBAR) filters. In the present work, single crystalline $LiNbO_3$ thin films are transferred by crystal ion slicing. Instead of the often used silicon dioxide, Benzocyclobutene is used as the bonding layer, which significantly increases the tolerance of wafer bonding for the surface flatness, thus a patterned bottom electrode is easily buried underneath the $LiNbO_3$ thin film during the ions slicing process. More importantly, this single Benzocyclobutene layer also acts as an effective acoustic reflector, and a large k_t^2 exceeding 21% is obtained in the LN-based bulk acoustic wave resonator. The Mason model is built up according to the experimental results, and the fitting shows that the Benzocyclobutene has a low acoustic impedance, which effectively confines the acoustic energy within the piezoelectric layer and results in the high k_t^2.

1. Introduction

RF filters are the most important passive devices in the RF front-end module for the applications in mobile communications. Bulk acoustic wave (BAW) filters with low insertion loss, high out-of-band rejection, compact size have been the mainstream solutions for those bands above 2.5 GHz.[1,2] A BAW filter is constitute of several BAW resonators, which have a parallel capacitor-like structure. The piezoelectric layer sandwiched by two electrodes, converting electrical energy into mechanical energy and vice versa, plays a decisive role on the performance of the BAW resonator and filter. Nowadays, all of the commercially available BAW filters are utilizing AlN or AlScN thin films as the piezoelectric layer.[3–5] However, even though the Sc doping dramatically increases the electromechanical coupling coefficient (k_t^2) of AlN to ∼15%, the resulted filter bandwidth of ∼7.5% still does not fulfill the future requirements of 5 generation mobile communication systems. Moreover, a high Sc doping level is not easy to achieve due to the composition segregation, and the doping also deteriorates the out-of-band rejection of the filter.[6,7]

$LiNbO_3$ (LN) crystal has been proven to exhibit much larger k_t^2 than AlN or AlScN, however, the k_t^2 of LN is strongly dependent on the orientation of the LN crystal.[8] Baron et al. has calculated the k_t^2 of longitudinal mode for YX-cut LN, and the results indicated that a very large k_t^2 above 30% can only be achieved in a YXl-36 cut LN plate.[9] Unfortunately, there is no chance to obtain a LN thin film with such a special orientation on metal bottom electrode by traditional thin film deposition techniques. Alternatively, the layer transfer technique involving wafer bonding and grinding has shown much flexibility for the fabrication of those crystals having special orientations. By transferring a YXl-36 LN thin plate onto a substrate, BAW resonators have been fabricated and k_t^2 as large as 20% has been achieved in a cavity-type resonance geometry.[10] Nevertheless, the LN layer thinned by mechanical grinding and polishing has a very large thickness of 10 μm, resulting in a resonance frequency in MHz range, which is far below the 4G or 5G working bands.

According to the longitudinal acoustic speed of ∼7400 m s^{-1} in YXl-36 LN, a BAW resonator working at a frequency above 2.5 GHz needs a LN layer with a thickness below 1500 nm, which is a challenge task for the mechanical grinding process. Therefore, a thin film transfer process adopting ion slicing has been developed to fabricate micron or sub-micron thick LN thin films. For example, Pijolat M. et al. obtained X-cut single crystal films of LN through SMART CUT™ technology.[11] Based on this technique, LN thin film resonators working at GHz range have been fabricated using various oriented LN layer. Osugi, Yukihisa et al. used thin film deposition to prepare single crystal LN FBAR in 2007.[12] Subsequently, M. Pijolat et al. fabricated a single crystal LN FBAR using direct bonding techniques.[13] In 2011, B. Imbert et al. used SMART CUT™ to obtain a Characterized film to prepare single crystal LN FBAR.[14] However, those resonators are working at high overtone mode as HBAR, which does not have an air gap (FBAR) or a Bragg reflector (SMR), differing from the BAW devices widely used in wireless communications.

The difficulty to fabricate LN-BAW devices is that the thin film transferring process involves a wafer bonding step, which needs very flat bonding surfaces. Usually the bonding medium is SiO_2, and a chemical mechanical planarization (CMP) on the SiO_2 layer is necessary before the bonding. However, a BAW resonator contains an air gap or a Bragg reflector, and the bottom electrode needs patterning, which produce large fluctuation on the wafer surface, making the process much more complicated.[15]

In the present work, sub-micron thick YXl-36 LN thin films are transferred by ion slicing technique, and a fluidic benzocyclobutene (BCB) layer is adopted as the bonding medium. The replacement of SiO_2 by BCB significantly increase the tolerance of wafer bonding for the surface flatness, thus a patterned bottom electrode is easily buried underneath the LN thin film during the ions slicing process. More importantly, due to the small acoustic impedance of

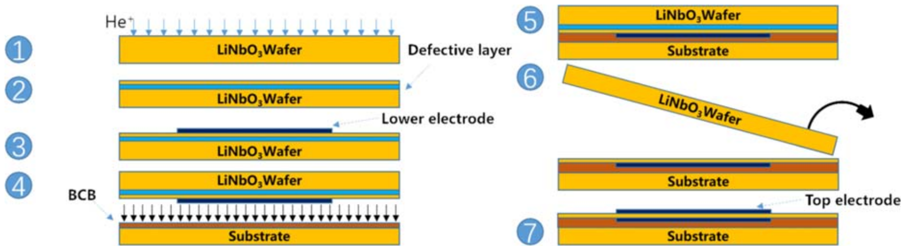

Fig. 1. (Color online) LN-BAW resonator preparation process.

BCB, this single BCB layer also acts as an effective acoustic reflector, and a large k_t^2 exceeding 21% is obtained in the LN-based BAW resonator. The performance of the resonators using different wafer bonding mediums of BCB and SiO_2 are finally compared in a Mason model.

2. Experimental methods

The process for the LN-BAW resonator is illustrated in Fig. 1. He^+ ions are implanted into a 4 inches YXl-36 LN wafer using an energy of 285 keV, which resulted in a defective layer at a depth of ~930 nm inside the LN wafer. The dose of the He^+ ions has been optimized to be 4×10^{16} ions cm^{-2}. Where after, an Al layer with a thickness of 100 nm is sputtered onto the implanted LN surface and patterned by photolithography, which will be the bottom electrode for the resonator. Another YXl-36 LN wafer is spin-coated with BCB and bonded to the implanted LN wafer after prebaking the BCB at 150 °C for 5 min. Since the prebaked BCB layer is at a semi-cured state, the patterned electrodes are embedded into the BCB layer under the bonding pressure. The bonded wafer pair is subsequently annealed in a vacuum oven at a temperature of 320 °C for 3 h. During the annealing, the BCB layer is fully solidified to achieve a very large bonding strength, meanwhile, the implanted LN wafer splits off and leave the LN thin film with patterned Al bottom electrodes on the LN substrate. Finally, patterned Al electrodes are fabricated on top of the LN thin film, and LN-BAW resonators with a BCB acoustic reflector are formed.[16,17]

3. Results and discussion

According to the process in Fig. 1(a), the solidification of BCB and the exfoliation of LN thin film take place simultaneously. Because the BCB layer transforms from a fluidic state to a solid state, the LN film is subjected to a dramatic change of strain imposed by the BCB. To examine the quality of the transferred LN thin film, θ–2θ scan and ω-scan by XRD are carried out on the film. Note that the sample for XRD measurement is not using LN as the substrate, instead, in order to obtain diffraction signal from the LN film and prevent the interference from the substrate, another YXl-36 LN thin film without electrode is transferred to an amorphous glass substrate by BCB bonding. The θ–2θ scanned pattern of the LN/glass is shown in Fig. 2(a), where only the peaks corresponding to the (012), (024) and (036) of planes are present, indicating the single crystalline nature of the thin film. The ω-scan is shown in Fig. 2(b), the peaks have a full width at half maximum of 0.0619°, indicating good crystal quality of the LN film.[18] It can be seen from the XRD test results that the crystal structure of the LN film is little damaged by He^+ ions. However, He^+ ions may form point defects in the LN film to cause a decrease in the k_t^2. In addition, the thin film thickness is confirmed by the cross sectional image of SEM, as shown in Fig. 2(c). The LN film and the BCB layer have a thickness of 932.5 nm and 0.6848 μm, respectively. The thickness of the LN film is in good agreement with the depth of the defective layer, which is determined by the implantation energy of 285 keV. While the thickness of the BCB layer is much larger than that of the Al bottom electrode, which can fully compensate the fluctuation on the wafer surface caused by the electrode patterning.

Based on this high quality LN thin film, a single port BAW resonator with BCB reflective layer is fabricated following the process in Fig. 1. The top electrode has a G-S-G geometry for microwave measurement, as shown in Fig. 3(a). The bottom electrode is connected to the top ground by depositing Al into the via, which is prepared by etching through the LN thin film using Ar^+ ions. The S11 coefficient is shown in Fig. 3(d), the return loss of the resonator is –7.488 dB at 3.040 GHz. The impedance curve indicates that the resonance frequency and anti-resonance frequency are 2.779 GHz and 3.051 GHz, respectively [Fig. 3(e)]. The impedance ratio is the ratio of the impedance at the resonant frequency to the impedance at the anti-resonant frequency, and the value of this device is 28.683 dB. Note that the resonator does not show obvious spurious modes in a wide frequency range of 1–5 GHz, indicating a pure longitudinal resonance mode in the device. The smith chart shows that the circle is relatively smooth.

The k_t^2 of the BAW resonator can be calculated by $K_t^2 = \frac{\Pi^2(f_a - f_r)}{4 \times f_a}$, where f_a and f_r donate to the resonance frequency and anti-resonance frequency, respectively.[19] Based on the result in Fig. 3(e), the k_t^2 of the YXl-36 LN thin film is 21.997%, which is about three times larger than that of AlN or ZnO thin film, and is also higher than the mechanical polished YXl-36 LN thin plate reported by Baron et al.[20,21] The k_t^2 of the test device is slightly smaller than the theoretical value. This indicates that He^+ ions passing through the LN film has little effect on the k_t^2. The large k_t^2 is owing to the high quality single crystalline LN thin film obtained by ion-slicing technique. In addition, the acoustic reflection realized by the BCB bonding medium confines the acoustic energy within the resonator and also contributes to the large k_t^2. The formula for calculating the Q value is $Q = \frac{f}{2}\left|\frac{\partial < \mathrm{Zin}}{\partial f}\right|_{f_a}$. The series resonance Q value Q_s and parallel resonant Q value Q_p are calculated to be 34.455 and 128.171, respectively.

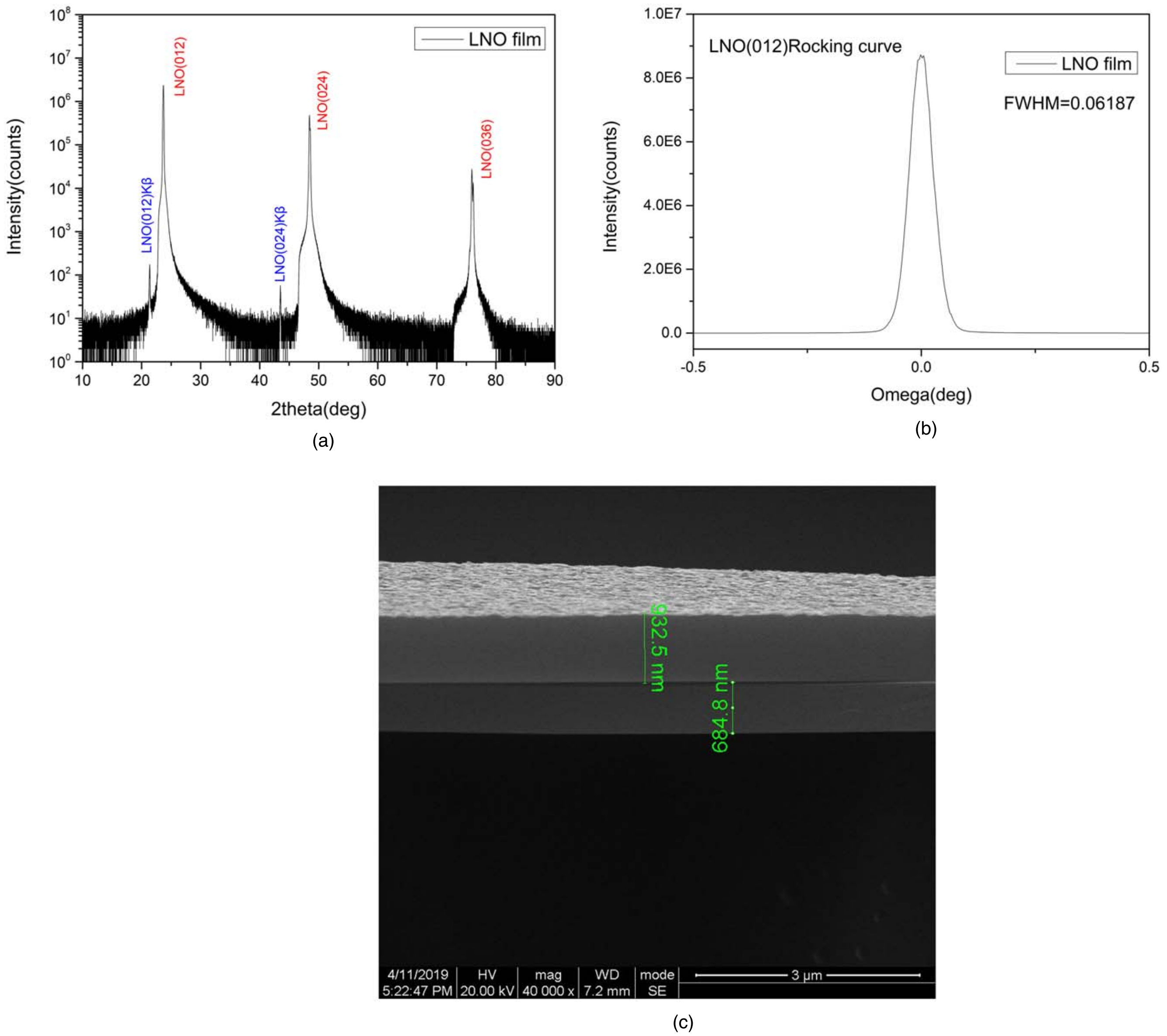

Fig. 2. (Color online) (a) The θ–2θ scanned pattern of the LN/glass. (b) The ω-scan of the LN/glass. (c) Cross-sectional images of LN-BAW resonator.

To further elucidate the function of BCB layer, Mason models are built up and various resonator structures are compared and evaluated [Fig. 3(b)].[22,23] The Mason model is established using the structural parameters of the test device and the ideal parameters of the corresponding materials. The parameters of the acoustic impedance, dielectric constant and acoustic loss of various materials are added to the model to simulate the working state of the device as much as possible. There are some interference factors in the actual device such as electrode quality and the presence of impurities and pores in the bonding layer of BCB. Therefore, some material parameters in the model are appropriately adjusted to better match the test data. The fitting results are shown in Fig. 3. It can be seen that the Mason model is in good agreement with the key parameters in the test data. Subsequently, some material parameters of BCB and LN film are extracted from the Mason model. The formula for calculating the acoustic impedance is $\mathrm{Zin} = \rho \times V$. The ρ is the density of the material and V is the speed of sound of the material. The BCB has a sound velocity of $2260\ \mathrm{m\,s^{-1}}$ and density of $1050\ \mathrm{kg\,m^{-3}}$. Theoretical value of BCB acoustic impedance is 2.373×10^6, but the fitting result is slightly lower than this.[24] The main reason for this phenomenon is that BCB forms some micropores during the curing process. Moreover, the contact loss and dielectric loss of LN are 4.263 Ω and 0.49 Ω, respectively. These two values were obtained by fitting the test data with the MBVD model. The contact loss is the overall equivalent of the loss of the resistance of the electrode and the loss of the external circuit contact in the Mason model.

Considering the fact that SiO_2 is much more often used as the bonding medium for ion-slicing technique, in spite of the complex processing before bonding, the device structure using SiO_2 as acoustic reflector is evaluated in Mason model as well. Besides, a reference device using the traditional W/SiO_2 as reflector is also simulated with Mason model and compared.[25] The resulted parameters obtained from the Mason models are summarized in Table I.

The Mason model with SiO_2 as the reflective layer was established under the condition of constant dielectric loss and contact loss (Fig. 4). First, the thickness of the SiO_2 layer is adjusted so that the parallel resonance frequency is consistent with the ideal case, and the minimum SiO_2 thickness is

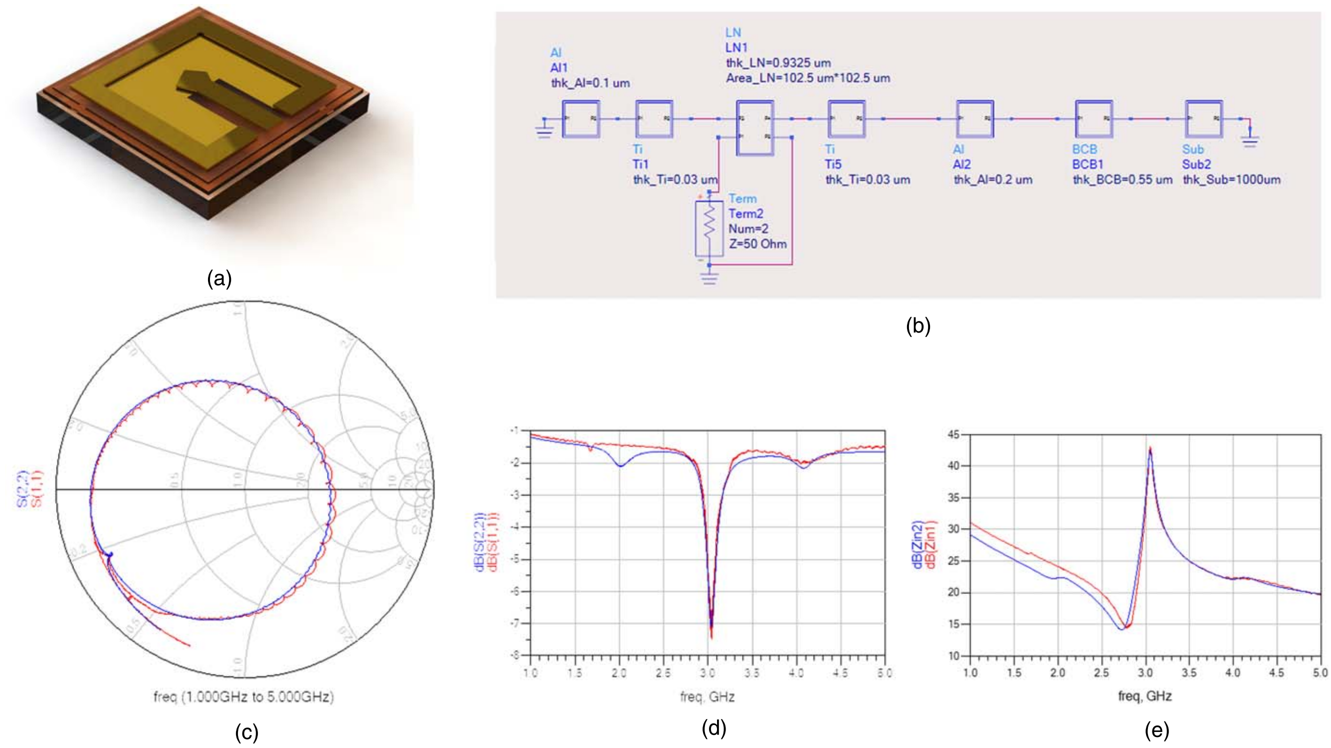

Fig. 3. (Color online) The red line in the figure is the test data and the blue line is the Mason model simulation data. (a) Schematic diagram of LN-BAW resonator. (b) Mason model circuit diagram. (c) Smith chart. (d) Return loss curve of LN-BAW resonator from 1 to 5 GHz. (e) Impedance curve.

Table I. Parameters of LN-BAW resonator devices with various reflective layers.

	Test data	BCB Mason model	SiO_2 Mason model	SiO_2-W Mason model
Contact loss (Ω)	—	4.263	4.263	4.263
Dielectric loss (Ω)	—	0.490	0.490	0.490
Acoustic impedance	—	2.305×10^6	1.250×10^7	$1.250 \times 10^7/1.06 \times 10^8$
dB(Zin_a/Zin_r)	28.683	28.439	11.072	36.918
Q_p	128.171	70.900	7.370	139.097
Q_s	34.455	18.900	4.941	17.123
Return loss	−7.488	−7.511	−10.248	−2.454

0.491 μm. This thickness of SiO_2 conforms to $\lambda/4$ (λ is the wavelength of sound waves) in sound wave transmission, and has the best reflection effect. In this case, the Q value is still very small, Q_s and Q_p are 4.941 and 7.370. The impedance ratio is also small, only 11.072 dB.[26] This shows that $\lambda/4$ thickness of a single SiO_2 layer does not have the good effect on the acoustic reflection. It can be seen from Fig. 4(b), there are a large number of hetero phases on the Smith circle. Those hetero phases cause a shift in the resonant frequency. A number of different Mason models of SiO_2 thickness are then obtained, while ensuring that the parallel resonant frequency is consistent with the ideal. The device parameters of the SiO_2 reflective layers of different thicknesses are collectively shown in Table II.

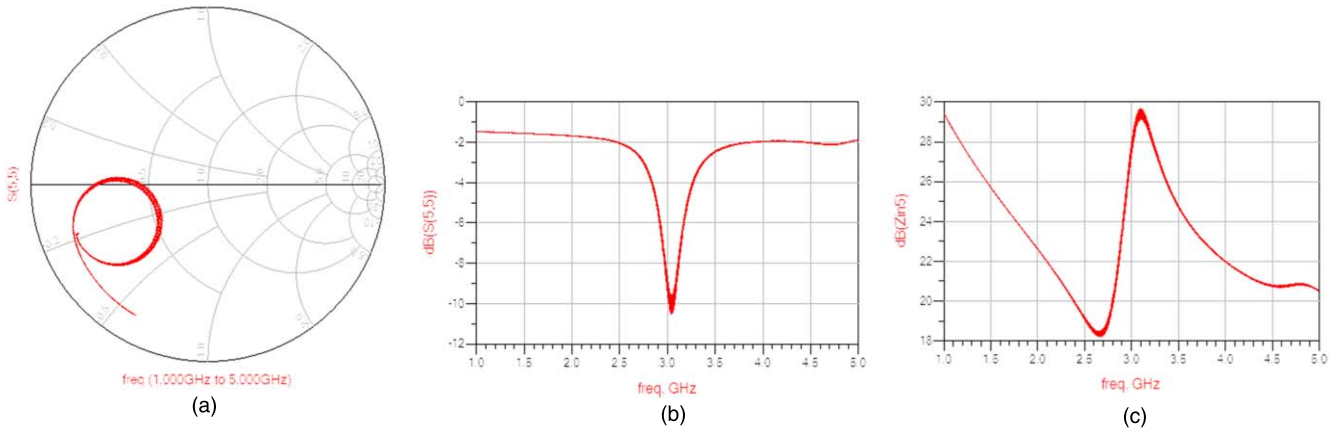

Fig. 4. (Color online) Simulation of Mason model with 0.491 μm SiO_2 as reflection layer. (a) Smith char. (b) Return loss curve from 1 to 5 GHz. (c) Impedance curve.

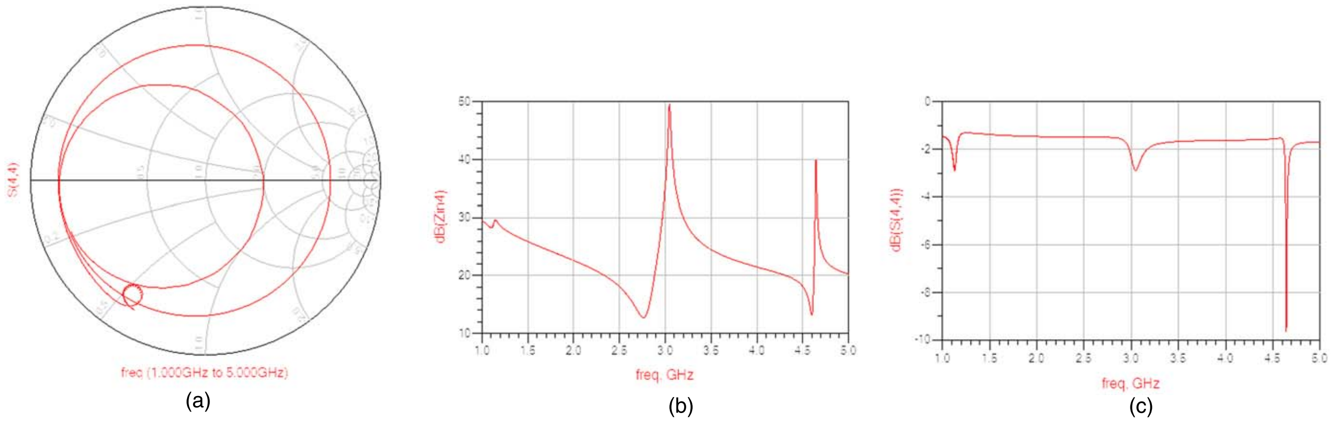

Fig. 5. (Color online) Simulation of Mason model with SiO_2-W as reflective layer. (a) Smith chart. (b) Return loss curve from 1 to 5 GHz. (c) Impedance curve.

Table II. Analog device parameters of Mason model with 0.491–5.129 μm SiO_2 as reflection layer.

SiO_2 thickness; (μm)	dB(Zin_a/Zin_r)	Parallel resonant Q value (Q_p)	Series resonance Q value (Q_s)	Return loss
0.491	11.072	7.370	4.941	−10.248
1.410	11.125	9.819	6.746	−10.460
2.346	11.218	12.632	8.616	−10.493
3.273	11.148	13.761	10.740	−10.512
4.199	11.111	15.187	13.593	−10.531

As the thickness of SiO_2 increases, the impedance ratio is always around 11 dB and many unwanted clutter appears. This phenomenon does not occur in devices where the BCB acts as a reflective layer. This is mainly due to the fact that BCB is a material with low acoustic impedance, which is an order of magnitude smaller than SiO_2, and BCB has higher loss, so it can still get a smoother impedance curve without the BCB thickness being precisely controlled at the ideal parallel resonant frequency thickness. BCB can achieve better reflection than SiO_2, does not lead to many peaks, and has a larger impedance ratio and Q value.

The device with BCB acoustic reflector is also compared with the one with SiO_2-W reflector, which is the most popular Bragg reflector used widely. The Mason model was established using a Bragg acoustic mirror of SiO_2-W as the reflective layer and compared with the test parameters (Fig. 5). The model's impedance ratio is 36.918 dB. The impedance ratio is not much different from that of BCB as a reflective layer. This indicates that while simplifying the complex fabrication process of the Bragg reflective layer, BCB can effectively ensure device performance.

Note that the simulation result with SiO_2-W as reflector still does not show very high Q factor, this is because a large contact loss and a dielectric loss are used in the model, which are deduces from the test results. The surface of the LN single crystal film prepared by ion implantation has a damaged surface layer, which has a large surface roughness of ~10 nm. The rough surface results in the leak of acoustic energy at the surface, thus the Q factor of the device is limited. However, an improved Q factor is expected after removing this damage layer by ion irradiation processing or CMP, which will be further investigated in the next.[27]

4. Conclusions

In this work, it has shown that the feasibility of the high-performance Y36 single crystal LN thin film BAW resonator was theoretically verified by simulation, and the LN-BAW with reliable performance was actually fabricated, with the use of BCB as acoustic reflective layer as the main innovation. Y36 cut single crystal LN film provides extremely high electromechanical coupling coefficient for the resonator, and BCB is an excellent low acoustic impedance material with good reflection effect. Although there are some interference factors, the effective electromechanical coupling coefficient of the LN-BAW we made are still as high as 21.997%, and the impedance ratio is 28.683 dB. In the future, the BCB thickness will be improved and the LN damage layer will be eliminated to prepare a better performance BAW resonator, which further reduces the manufacturing cost of the RF filter device and improves the performance of the RF filter device.

Acknowledgments

This work was supported by the National Key Research and Development Plan (2017YFB0406400) and National Natural Science Foundation of China (Nos. 51772044, 51602039, U1435208).

1) K. Katsalis, N. Nikaein, E. Schiller, A. Ksentini, and T. Braun, IEEE Commun. Mag. **55**, 146 (2017).
2) P. Popovski, 1st Int. Conf. on 5G for Ubiquitous Connectivity (Akaslompolo, Finland), p. 146.
3) R. Lanz, M. Dubois, and P. Muralt, 2001 IEEE Ultrasonics Symp. Proc. An Int. Symp., 2001 (Atlanta, GA, USA),Vol. 1, p. 843.
4) V. Pashchenko, R. Matloub, F. Parsapourkolour, P. Muralt, S. Ballandras, and K. Haffner, 2016 IEEE Int. Ultrasonics Symp., 2016 (Tours, France), p. 1.
5) C. L. Wei, Y. C. Chen, C. C. Cheng, K. S. Kao, C. J. Chung, and W. T. Chang, Mater. Sci. Forum **654–656**, 1792 (2010).
6) H. Bartzsch, G. Suchaneck, and G. Gerlach, Spie Microtechnologies, Smart Sensors, Actuators, and MEMS VII; and Cyber Physical Systems, 2015 Vol. 9517, p. 951704.
7) T. Yanagitani, K. Arakawa, K. Kano, A. Teshigahara, and M. Akiyama, 2010 IEEE Int. Ultrasonics Symp., 2011 (San Diego, CA, USA), p. 2095.
8) Y. Fujiwara and N. Wakatsuki, IEEE Trans. Ultrason. Ferroelectr. Freq. Control **34**, 39 (1987).
9) C. Lise, G. Sylvain, C. Matthieu, B. Stéphane, C. Dominique, B. Thomas, B. Sylvain, E. Laetitia, and M. Philippe, Int. J. RF Microwave Comput. Aided Eng. **21**, 458 (2011).
10) M. E. Hakiki, J. A. Damy, H. Hartmann, J. M. Brice, and X. Perois, 2011 IEEE Int. Ultrasonics Symp., 2012 (Orlando, FL, USA), p. 1325.

11) M. Pijolat, A. Reinhardt, E. Defay, C. Deguet, and S. Ballandras, Proc. of the IEEE Ultrasonics Symp., 2008, p. 201.
12) Y. Osugi, T. Yoshino, K. Suzuki, and T. Hirai, 2007 IEEE/MTT-S Int. Microwave Symp., 2007 (Honolulu, HI, USA), p. 873.
13) P. Multarzyński, IEEE Int. Frequency Control Symp., 2010 Vol. 29, p. 661.
14) B. Imbert, A. Reinhardt, T. Ricart, C. Billard, M. Pijolat, E. Defay, E. Augendre, T. Signamarcheix, and C. Deguet, 2011 Joint Conf. of the IEEE Int. Frequency Control and the European Frequency and Time Forum (FCS) Proc., 2011 (San Francisco, CA, USA), p. 1.
15) H. Ran, M. Fujino, A. Yamauchi, and T. Suga, Jpn. J. Appl. Phys. **55**, 04EC02 (2016).
16) G. Poberaj, M. Koechlin, F. Sulser, A. Guarino, J. Hajfler, and P. Günter, Opt. Mater. **31**, 1054 (2009).
17) A. Guarino, G. Poberaj, D. Rezzonico, R. Degl'Innocenti, and P. Günter, Nat. Photonics **1**, 407 (2007).
18) I. Kashif, A. A. Soliman, E. M. Sakr, and A. Ratep, Spectrochim. Acta A **113**, 15 (2013).
19) J. D. L. Iii and Y. Oshrnyansky, 2002 IEEE Ultrasonics Symp., 2002. Proc., 2002 (Munich, Germany), Vol. 1, p. 939.
20) Y. Satoh, T. Nishihara, T. Yokoyama, M. Ueda, and T. Miyashita, Jpn. J. Appl. Phys. **44**, p. 2883 (2005).
21) T. Baron, J. Masson, J. P. Romand, S. Alzuaga, L. Catherinot, M. Chatras, and S. Ballandras, EFTF-2010 24th European Frequency and Time Forum (Noordwijk, Netherlands), p. 1.
22) M. El Hassan, E. Kerherve, Y. Deval, and D. Belot, 2007 IEEE/MTT-S Int. Microwave Symp., 2007 (Honolulu, HI, USA),, p. 1603.
23) Y. Shuai, Z. Yun, L. Sun, Z. Lian, C. Zhe, J. Wang, J. Li, Y. Shuai, Z. Yun, and L. Sun, 2016 13th China Int. Forum on Solid State Lighting: Int. Forum on Wide Bandgap Semiconductors China (SSLChina: IFWS), 2016 (Beijing, China), p. 120.
24) E. Martin, C. Larato, A. Clément, and M. Saint-Paul, NDT&E Int. **41**, 280 (2008).
25) T. Florian, H. Ken-Ya, O. Tatsuya, and Y. Masatsune, IEEE Trans. Ultrason. Ferroelectr. Freq. Control **57**, 2844 (2010).
26) R. Thalhammer and R. Aigner, IEEE Mtt-s Int. Microwave Symp. Digest, 2005 (Long Beach, CA, USA), p. 225.
27) X. Bai, S. Yao, C. Gong, C. Wu, W. Luo, R. Böttger, S. Zhou, and W. Zhang, Appl. Surf. Sci. **434**, 669 (2018).